The durability of adhesively joints in space structure during interplanetary exploration

Charpentier, G.V.M.; Lafont, Ugo; Teixeira De Freitas, S.

Publication date
2022

Document Version
Final published version

Published in
Proceedings of the 20th European Conference on Composite Materials: Composites Meet Sustainability

ECCM 20

26-30 JUNE 2022

LAUSANNE SWITZERLAND

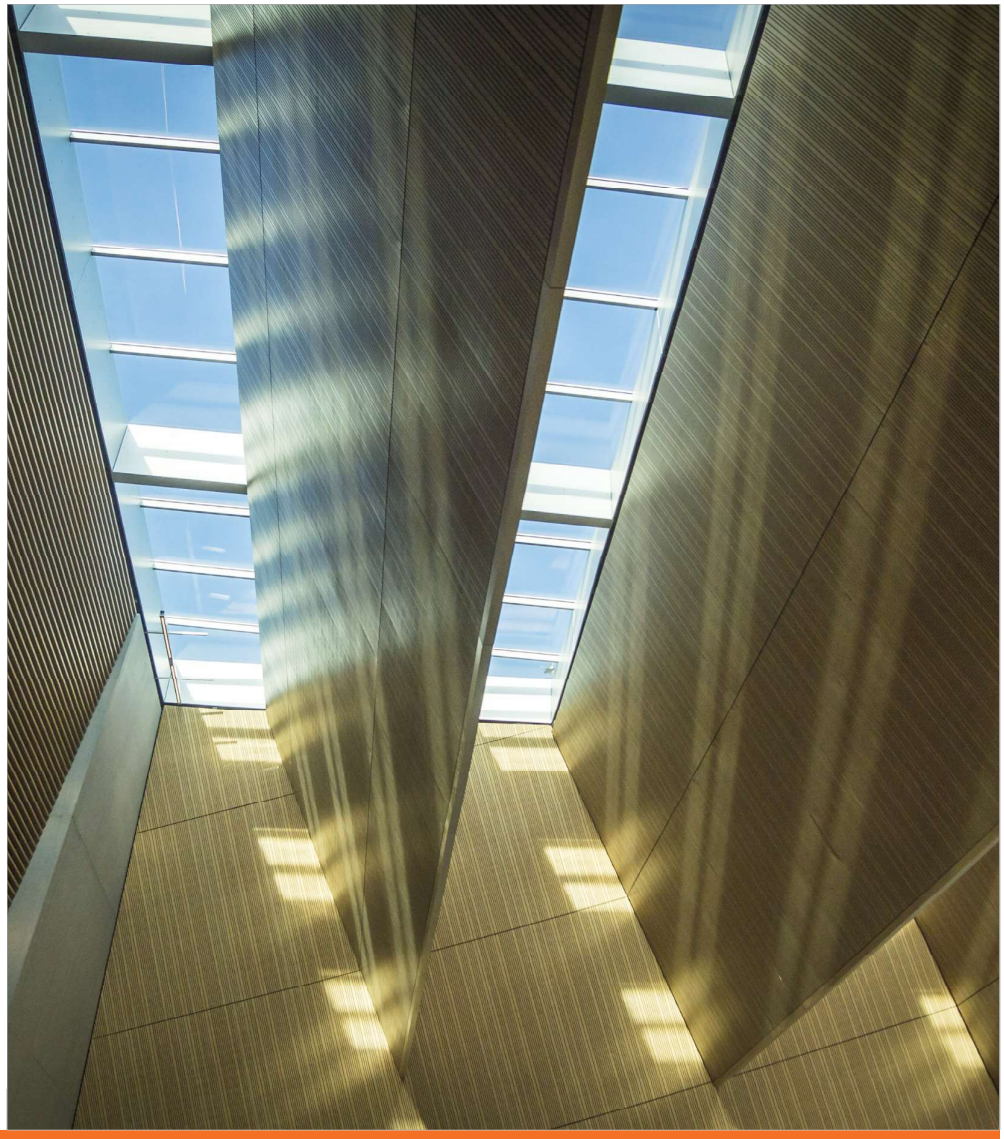

Proceedings of the 20th European Conference on Composite Materials

COMPOSITES MEET SUSTAINABILITY

Vol 2 – Manufacturing

Editors : Anastasios P. Vassilopoulos, Véronique Michaud

Organized by : EPFL CCLAB Composite Construction Laboratory

Under the patronage of : LPAC Laboratory for Processing of Advanced Composites; ESCM EUROPEAN SOCIETY FOR COMPOSITE MATERIALS

ECCM 20
26-30 JUNE 2022
LAUSANNE SWITZERLAND

EPFL CCLAB Composite Construction Laboratory LPAC Laboratory for Processing of Advanced Composites

Proceedings of the 20th European Conference on Composite Materials ECCM20 26-30 June 2022, EPFL Lausanne Switzerland

Edited By :

Prof. Anastasios P. Vassilopoulos, CCLab/EPFL
Prof. Véronique Michaud, LPAC/EPFL

Oragnized by:

Composite Construction Laboratory (CCLab)
Laboratory for Processing of Advanced Composites (LPAC)
Ecole Polytechnique Fédérale de Lausanne (EPFL)

ISBN: 978-2-9701614-0-0
DOI: http://dx.doi.org/10.5075/epfl-298799_978-2-9701614-0-0

Published by :

Composite Construction Laboratory (CCLab)
Ecole Polytechnique Fédérale de Lausanne (EPFL)
BP 2225 (Bâtiment BP), Station 16
1015, Lausanne, Switzerland

https://cclab.epfl.ch

Laboratory for Processing of Advanced Composites (LPAC)
Ecole Polytechnique Fédérale de Lausanne (EPFL)
MXG 139 (Bâtiment MXG), Station 12
1015, Lausanne, Switzerland

https://lpac.epfl.ch

Cover:

Swiss Tech Convention Center
© Edouard Venceslau - CompuWeb SA

Cover Design:

Composite Construction Laboratory (CCLab)
Ecole Polytechnique Fédérale de Lausanne (EPFL)
Lausanne, Switzerland

©2022 ECCM20/The publishers

Disclaimer:

THE DURABILITY OF ADHESIVELY JOINTS IN SPACE STRUCTURE DURING INTERPLANETARY EXPLORATION

Gabin, Charpentier [a,b], Ugo, Lafont [c], Sofia, Teixeira De Freitas [a]

a: Faculty of Aerospace Engineering, Delft University of Technology, Kluyverweg 1, 2629 HS Delft, The Netherlands
b: ISAE ENSMA, Téléport 2, 1 Avenue Clément Ader, BP 40109, 86961 Futuroscope Chasseneuil, Cedex, France
gabincharpentier@gmail.com
c: European Space Agency, Keplerlaan 1, PO Box 299, 2200 AG Noordwijk, The Netherlands – ugo.lafont@esa.int

Abstract:

Spacecraft are subjected to very few mechanical loads but in the future with reusable spacecraft designed for interplanetary explorations and with the repetition of landing and takeoff, structures will be subjected to increased mechanical loads. The effect of space environment on the aging of adhesive materials used as joints in space structure is not well understood for such long-term application. In this study, two adhesives widely used in spacecraft assembly were investigated: Scotch-Weld™ EC-2216 and Scotch-Weld™ EC-9323-2. They were subject to two aging conditions: (1) high energetic electron irradiation using a Van de Graaf accelerator and (2) thermal vacuum cycling. The results related to the evolution of the intrinsic adhesive properties and adhesion to CFRP and aluminum adherents were investigated before and after environmental exposure with tensile tests, peel tests, double cantilever beam (DCB) tests and dynamic mechanical analysis (DMA).

Keywords: Adhesives; space environment; aging

1. Introduction

Spacecraft and satellites are subjected to very few mechanical loads in space, but in the future with reusable spacecraft, loads can become significant. Indeed, for spacecraft designed for interplanetary explorations and with the repetition of landing and take-off (on the Moon or Mars or some asteroids for instance) [1-2] the structure will be subject to more repetitive mechanical loads and thus even after long period of exposure toward space environment.

In such conditions, materials intrinsic properties will evolve. One of the first effect related to exposure to space vacuum is outgassing. Due to the vacuum, molecules from an organic component tend to be released into space [3-5]. However, minimizing and controlling such effect is mainly driven by the need to avoid molecular contaminants that can be release and later re-adsorbed by sensitive surface of a spacecraft like optics. Outgassing can be anticipated and countered prior to launch with using material that have very low outagassing and implementing bakeout strategy on ground prior launch phase. At this stage, the integrity of adhesives are not impacted by outgassing and can be discarded as relevant parameter. Radiation is also an integral part of the special conditions to which spacecrafts are subjected. This radiation

  doi:10.5075/epfl-298799_978-2-9701614-0-0

is broken down over the entire spectrum of light depending on the wavelength. Thus, a material expose to space is subjected to two types of radiation: energetic photons (UV-ray, X-ray, γ-ray) which come from the solar flux and charged particle (electrons, protons, nucleon) trapped by electromagnetic fields such as the van Allen belt around the earth [6]. The effect of different types of radiation on the materials mechanical properties may vary in the case of polymers. Radiation causes molecular chain scission and recombination or cross-linking in macromolecular chain leading to deformation, embrittlement, and discoloration, which affect the mechanical integrity of the polymer [7-8]. Another parameter of the space environment, specific to Low Earth Orbit and able to induce degradation of the materials is Atomic Oxygen (ATOX). Oxygen atoms are generated during the photo-dissociation of the oxygen molecules of the atmosphere by the solar electromagnetic radiation [7] leading to the breaking of the bond between two atoms. These very reactive species can interact with the surface of any exposed material and degrade it. Even if Atomic Oxygen is mostly present around Earth it can also be produced in other planetary environments, such as the Mars orbital environment, where oxygen is also present. It should be notice that although the effects of ATOX can induce severe material degradation like etching, pitting, it will not be considered in this study as adhesives are generally protected from direct exposure to atomic oxygen and are therefore not affected by this space environmental factor.

In terms of temperature, the space environment goes from very low to very high temperatures, so the adhesive must be resistant to its use [8-9]. With temperature gradients, thermal residual stresses can occur at the bond line between materials with different coefficients of thermal expansion. This can create stresses and therefore failures, damage, delamination, etc.

Furthermore, as detailed in the literature, one of the major issues related to adhesives is the differentiation between adhesion and material properties of the adhesive. On the one hand, adhesion represents the force that bonds a material to the adhesive and can be quantified through various adhesion mechanical tests [10-11], such as peel tests. The intrinsic material properties of the adhesive, on the other hand, are mainly determined by physical-chemical and mechanical tests of the adhesive material itself [12].

The choice of adherent is another important issue for adhesives. Indeed, in most spacecrafts more and more composite materials such as CFRP are used, as well as metal such as aluminum which is still widely used because of its lightness [13-14]. The literature provides numerous mechanical parameters on the durability of adhesives in contact with these two types of surfaces, for unaged specimens or specimens subjected to hydrothermal aging. However, the literature remains rather poor in information on durability of adhesion subjected to space environment.

The durability of the adhesive materials used as joints in space structure is not yet known for spacecraft subjected to repeated launching loads and several phases of exposure to space conditions (for a 10, 15, 20, ... years exploration). Thus, the challenging question is to anticipate the mechanical and physico-chemical properties degradation of adhesives after X years. The literature has no precedent for the aging of certain material properties related to space conditions. Furthermore, there is lack of adhesion assessment in space aging environment, using mechanical and physical testing. This study will therefore aim to determine the durability of adhesion-related properties, under space environment such as fracture toughness, peel load and surface failure modes. In addition, material properties such as glass transition temperature,

  doi:10.5075/epfl-298799_978-2-9701614-0-0

young's modulus, tensile strength and strain at break will be investigated. The objective is to complement the literature by providing new data on the aging of adhesives for long-term space exploration application.

In this research, we looked into the effect of thermal vacuum cycling and high energetic electron irradiation on the properties of two adhesives that are widely used for space application Scotch-Weld™ EC-2216 and Scotch-Weld™ EC-9323-2. Adhesive behavior for Composite-to-composite and Alumimium-to-aluminum joints were evaluated using double cantilever beam tests (DCB) and floating roller peel tests (FRPT), respectively. The evolution of the adhesive intrinsic properties like tensile strength, thermo-mechanical behavior were investigated by means of tensile tests and Dynamic Mechanical Analysis (DMA).

2. Materials and Methods

2.1 Materials

Two types of adhesives were investigated: Scotch-Weld™ EC-2216 and Scotch-Weld™ EC-9323-2. Their respective processing/curing temperature and time and the mixing ration between the two parts are reported in Table 1. Both adhesives are space qualified but are used in different applications. Having a low Tg, EC-2216 is used for bonding elements that have no structural application at high temperatures while EC-9323-2, having a higher Tg, is used mainly in structural applications.

Table 1: Adhesive materials and corresponding curing cycle.

Adhesive	Curing temperature [°C]	Curing time [mm/min]	Part A/B [Weight ratio]
EC 2216	66	120	7/5
EA 9323-2	65	120	1/2

To assess the adhesion to CFRP, Double Cantilever Beam specimens were produced using carbon fibers already pre-impregnated with epoxy resin. CFRP were prepared from a unidirectional pre-preg consisting of Hexply 8552 epoxy matrix in combination with AS4 carbon fiber (Hexcel Corporation, Stamford, Connecticut, USA). To produce the two-rigid adherent of a DCB samples, a lay-up of 8 plies [0°]s of approximately 1.6 mm was used. The laminate was cured for 120 min at 180 °C. Prior to bonding, the cured CFRP surfaces were prepared by mean of abrasion with sand paper and cleaned with acetone.

To assess the adhesion to aluminum, floating roller peel test specimens were produced using clad Alumimium alloy 2024. The aluminum surfaces were pre-treated by grit blasting, coated with Sol-Gel 3M AC-130-2 and sprayed with 3M Scotch-Weld™ Primer 3901. The flexible aluminum sheets were 0.6 mm thick and the rigid aluminum sheets were 1.6 mm thick.

2.2 Methods

For tensile tests, experimental procedure was based on the standard test method for tensile properties of plastics described in ASTM D638 [15]. Testing was carried out using Zwick machine (Zwick, Ulm, Germany) equipped with a load cell of 1 kN. For EC-2216, the test speed was 5

mm.min^{-1} and the crosshead displacement and load were recorded each 5 s and 0.42 mm. For EC-9323-2, the test speed was 0.5 mm.min^{-1} (to ensure a similar acquisition time before failure as the EC-2216 because the EC-9323-2 is a more brittle adhesive that breaks more quickly at imposed displacement) and the crosshead displacement and load were recorded for all 5 s and 0.042 mm. Displacement data were recorded using a DIC (Digital Image Correlation) setup.

For Dynamic Mechanical Analysis (DMA), experimental procedure was based on the standard test methods for glass transition temperature, loss modulus and storage modulus determination as described in ASTM D7028, E2254 and E2425 [16-18]. Testing was carried out using TA Instrument RSA G2 machine (TA Instrument, New Castle, Delaware, USA) with a temperature range between -40°C and 140°C, a ramp rate of 2°C.min^{-1}. The test were performed in flexion mode (3 point bending).

For floating roller peel test (FRPT), the experimental procedure was based on the standard test method described in ASTM D3167 [19]. Testing was carried out using Zwick machine (Zwick, Ulm, Germany) coupled with a load cell of 1 kN. The testing speed was 125 mm.min^{-1}.

For Double cantilever Beam (DCB), test procedure follows the standard method of determining fracture toughness described in ASTM D5528 [20]. For this purpose, a Zwick machine (Zwick, Ulm, Germany) coupled with a load cell of 1 kN was used. The testing speed was 2 mm.min^{-1}. The crack length propagation in the bond line was monitored using millimetric paper and camera observation.

2.3 Sample preparation

DMA and tensile test specimens were produced via machining of plates of pure adhesive material. These plates were produced by placing adhesive between two glass plates with a control thickness of 2 mm and cured in an oven (as per Table 1). The plates were then machined to cut out specimens of 12 x 56 x 2 mm for DMA specimens as described in ASTM E2254 and ASTM E2425 [17-18] and 20 x 150 x 2 mm as per ASTM D638 standard [18] (Figure 1).

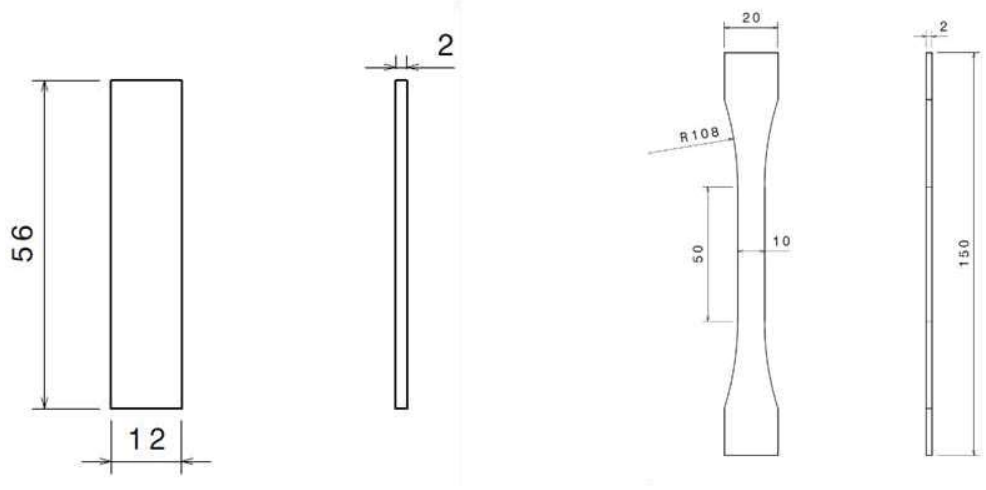

Figure 1: Sample shape and dimension for (Left) DMA and (Right) tensile testing

For FRTP specimens, after applying Teflon tape to the first 75 mm of the flexible adherent length (25 mm for the opening crack and 50 mm for the flexible adherent that protrudes from the rigid adherent, as shown on Figure 2). To control the adhesive bond line, 0.1% wt of glass beads of

250 microns in diameter were added to the mixture between part A and part B. The blend was then spread on the aluminum plates, which were then joined together using weights and cured in oven (as per Table 1). Floating roller peel test specimen dimensions were based on the standard test method ASTM D3167 [19] for floating roller peel resistance of adhesives. Specimens were 12.5 mm width and 350 mm long with a bond line thickness of 0.15 ± 0.05 mm.

For double cantilever beam specimens, Teflon tape was applied on the 50 mm of CFRP plates to create the crack opening, then similar glass beads were added with the same ratio as for floating roller peel test procedure and cured in an oven. Double Cantilever Beam specimen dimensions were based on the standard test method ASTM D5528 [20] for mode I interlaminar fracture toughness of unidirectional fiber-reinforced polymer matrix composites. Specimens were 25 x 220 mm with a 50 mm crack opening and a bond line thickness of 0.17 ± 0.06 mm.

Both aluminium-to-aluminium (FRTP test) and composite-to-composite (DCB test) products were then machined to cut out specimens with the desire dimension (Figure 2).

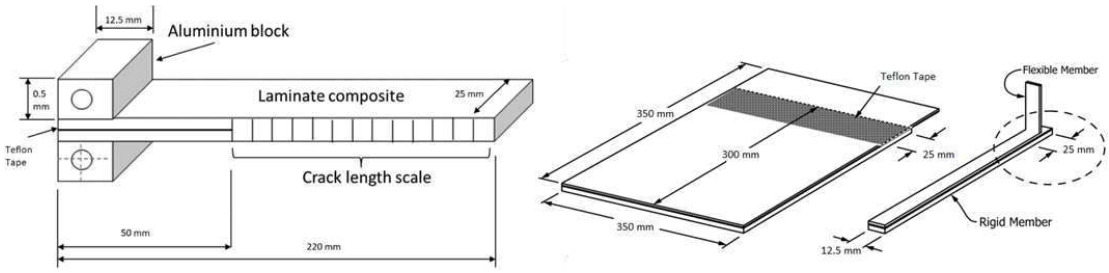

Figure 2: (Left) DCB and (Right) Peel test specimen dimension

2.3 Space environment exposure

In order to mimic space environment conditions, two different type of space environment were considered in this study: thermal vacuum cycling and irradiation with high energetic electrons. Thermal vacuum cycling test was carry out at ESA-ESTEC (Noordwijk, Netherlands) using a dedicated chamber for 25 cycles between -100°C and 100°C at 10^{-6} mbar. The period of each cycle was 4 hours and total duration was about 100 hours. Electron irradiation was performed at the Delft Reactor Institute (Delft, Netherlands) using a Van de Graaf accelerator. Samples were subjected to a total ionizing dose of 1 MGy using electron beam delivering 1.5 10^{12} $e^-.cm^{-2}.s^{-1}$ and an average dose of 47.4 $kGy.cm^{-2}$ for 3.5 h

For each characterization technique, five (N=5) specimens were tested per adhesive and configuration with the following conditions: (1) unaged/pristine, (2) after irradiation exposure and (3) after thermal vacuum cycling.

3. Results and Discussion

3.1 Effect space environment on adhesive intrinsic properties

In order to evaluate the aging effect on the adhesives, five parameters were derived from the experimental results: Young Modulus, Tensile strength and Strain at break (tensile tests), glass transition temperature (DMA and DSC tests) and heat flow (DSC tests).

Figure 3 shows the representative stress-strain curves obtained for both adhesives under the three conditions. The average values for Young's modulus, tensile strength and strain at break are given in Table 3.

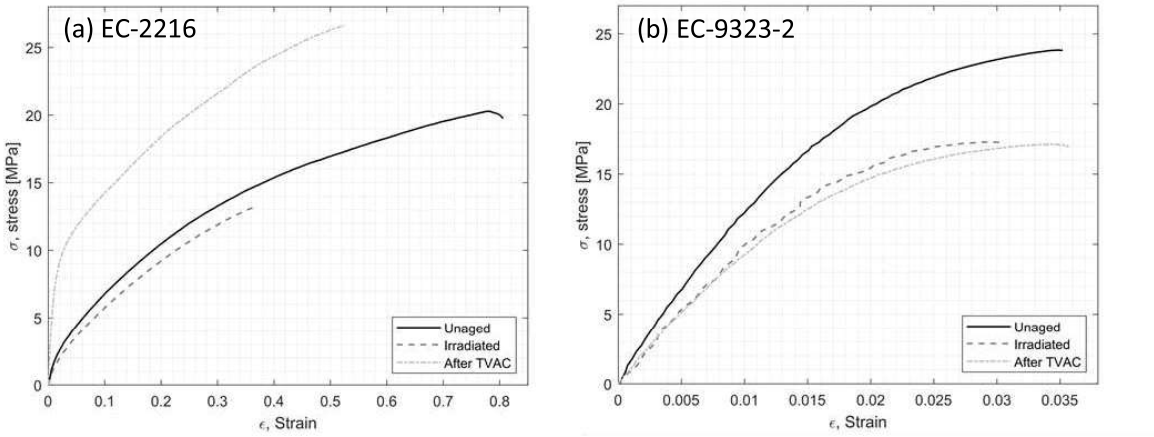

Figure 3: Typical tensile stress-strain of EC-2216 (Left) and EC-9323-2 (Right) as-produced (unaged), after irradiation and after Thermal vacuum cycling (TVAC)

For EC-2216 (Figure 3a) it can be noticed that behaviors are different after particle irradiation and TVAC. After particle irradiation the average Young's modulus drops from about 240 MPa for a non-aged sample to about 120 MPa for an irradiated sample. On the contrary, after Thermal Vacuum Aging Cycling (TVAC) the average Young's modulus increases to about 600 MPa. The stress-strain curve in its elastic zone, after TVAC, is much steeper in addition to presenting a larger elastic zone than for unaged material. This is also reflected in the tensile strength value that increases by almost 50% after TVAC, whereas it decreases by about 25% after irradiation. Finally, both types of aging have the same effect on elongation at break by decreasing its value, and therefore decreasing the ability of this adhesive to elongate prior to failure when subjected to tensile loading, even though particle irradiation decreases it more than TVAC. It is clear for EC-2216 that irradiation leads to a general decrease of the tensile properties whereas TVAC leads to an overall increase. Such improvement after TVAC can be attributed to a the post-curing effect occurring during the thermal cycling.

For EC-9323-2 (Figure 3b), the tensile behavior is similar after TVAC and particle irradiation. However, compare to the non exposed samples, modulus decreases by a factor 2 to from 2.2 GPa to 1.1 GPa for the pristine sample and the sample exposed to irradiation and TVAC, respectively. The same trend is observed in the tensile strength that also decreases after both aging conditions. The elongation of EC-9323-2 is almost unaffected after aging. However, the fracture surface of the sample reveals the presence of small voids for EC-9323-2 for all samples that were not present for EC-2216. Even if such inhomogeneity could have a negative effect on the general tensile properties, the EC-9323-2 tensile test reached a plateau as expected with respect to the mechanical behavior of such material. However, the strain might be not fully representative and shall not be considered. This difference of homogeneity between the 2 type of adhesive is related to the preparation process. In this study, the mixing process where identical for both adhesive and potentially not optimized. For space application, each bonding procedure is qualified and validated leading to a stable and reproducible process. This aspect

  doi:10.5075/epfl-298799_978-2-9701614-0-0

was not the focus of this study even if it is clear that is will have an impact on the optimum performance of the adhesive.

Table 2: Average tensile properties of EC-2216 and EC-9323-2 including standard deviation

Aging	Scotch-Weld™ EC-2216			Scotch-Weld™ EC-9323-2		
	E [MPA]	σ_{max} [MPA]	ε_{max}	E [MPA]	σ_{max} [MPA]	ε_{max}
Unaged	242 ± 48	19 ± 1.3	0.74 ± 0.08	2197 ± 703	20 ± 4.2	0.027 ± 0.007
Irradiated	123 ± 49	15 ± 3.3	0.53 ± 0.29	1026 ± 267	17 ± 2.2	0.026 ± 0.008
After TVAC	606 ± 130	28 ± 1.5	0.61 ± 0.07	1042 ± 198	18 ± 1.0	0.033 ± 0.008

DMA (Dynamical Mechanical Analysis) was performed to investigate the visco-elastic behavior and the glass transition temperature (Tg). The elastic storage modulus (E') which is proportional to the energy fully recovered per deformation cycle, the loss modulus which is proportional to the net energy dissipated in heat per cycle (E'') and tan δ the loss factor which represents the damping during dynamic deformation are plotted in Figure 4. The Tg was extracted at the temperature at which tan δ is maximum. Tg values are reported in Table 3.

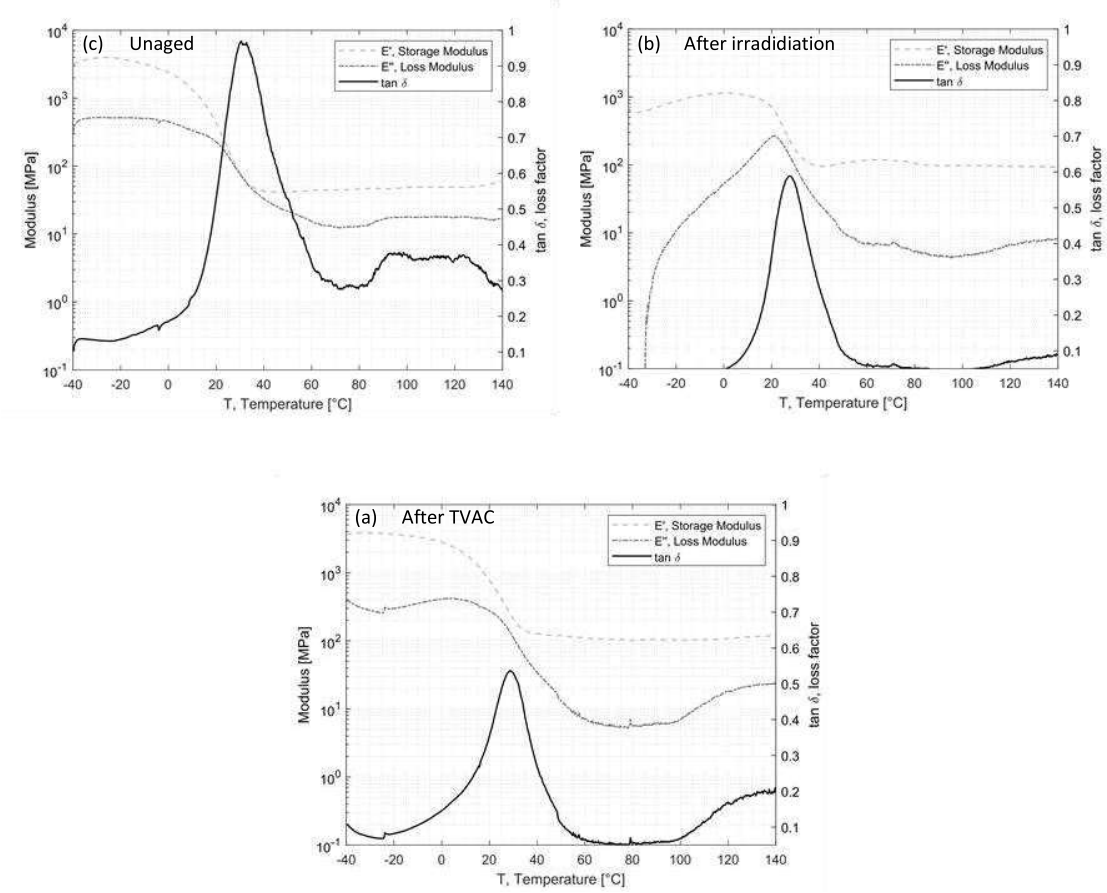

Figure 4: Evolution of storage and loss modulus, tan δ for EC-2216 (a) before aging and after (b) irradiation and (c) TVAC (c)

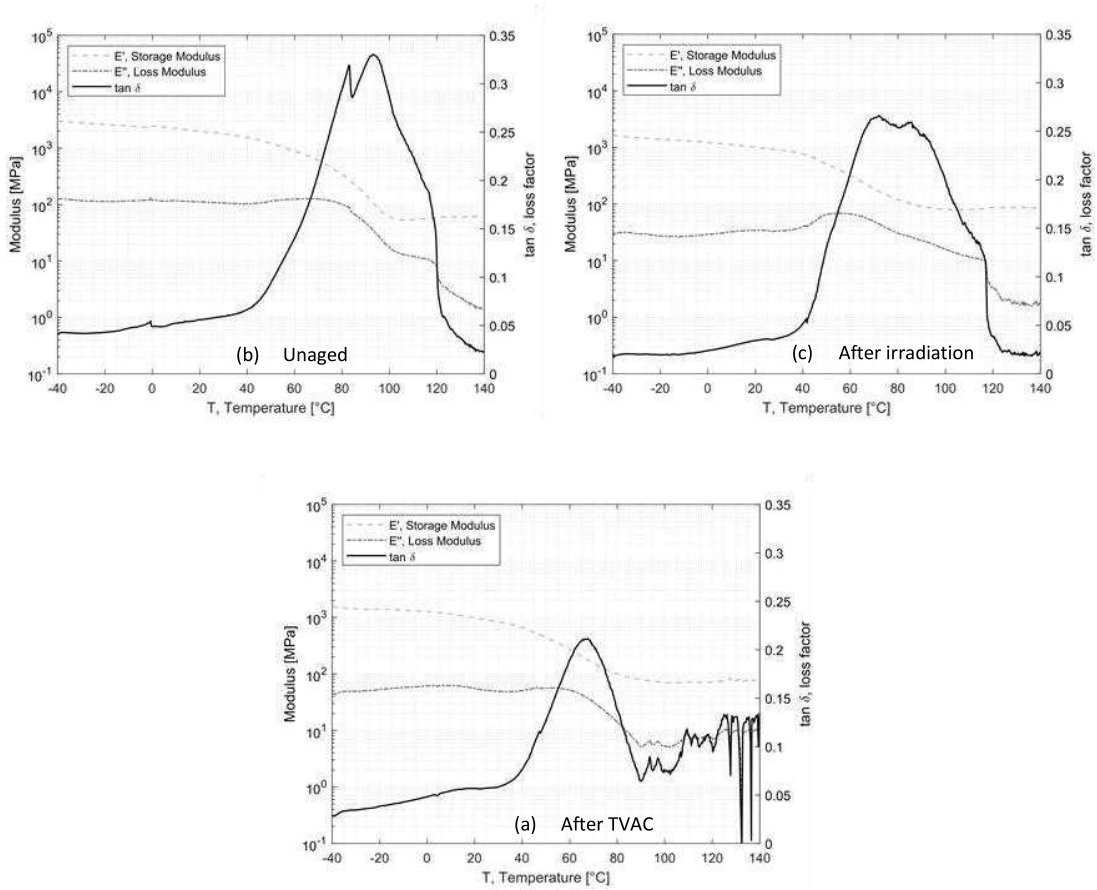

Figure 5: Evolution of storage and loss modulus, tan δ for EC-9323-2 (a) before aging and after (b) irradiation and (c) TVAC

Table 3: Average glass temperature evolution as function of the environmental exposure

Aging	T_g from max Tan δ [°C]	
	Scotch-Weld™ EC-2216	Scotch-Weld™ EC-9323-2
Non Aged	28 ± 1.1	91 ±7.4
Irradiated	30 ± 2.2	72 ± 3.6
After TVAC	30 ± 1.8	68 ± 7.8

For EC-2216, it can be seen that after irradiation or TVAC exposure the Tg increases by 2 °C in comparison to the pristine/unaged material. This change is not very significant taking into the standard deviation. However, the value of the maximum of tan δ which is around 1 for unaged sample, drops around 0.6 after TVAC and irradiation. This means that the ability of the adhesive to dissipate energy into heat after aging is lower. This could be explained by the average diminution of Loss Modulus with the aging. Indeed, in Figure 4b, it can be seen that after irradiation over the temperature range of -40 °C to 20 °C the loss modulus increases from almost zero to a peak at about 300 MPa, in contrast to unaged where it gradually decreases throughout

  doi:10.5075/epfl-298799_978-2-9701614-0-0

the temperature range. After TVAC, the loss modulus follows the same pattern as for unaged sample except that it increases significantly from 100 °C to 140 °C. These increases mean that over the relevant intervals the EC-2216 experiences an increase in net energy dissipated per cycle. The storage modulus, which is proportional to the total energy recovered per deformation cycle, does not change significantly after aging. It can also be noticed that the glassy state, the glass transition range and the rubbery plateau are not changing in a major way for unaged and irradiated sample as they are respectively between -40 °C and 0 °C, 0 °C and 60 °C, 60 °C and 100 °C. After TVAC (i.e. 25 cycles between -100 °C and 100 °C) the glass transition range is between -30 °C and 60 °C. Furthermore, the tan δ is decreasing between -40 °C and -30 °C which suggests a flow region for lower temperatures.

For EC-9323-2, the glass transition zone extends from 40 °C to 120 °C for unaged and irradiated samples. After TVAC, this range is again modified but this time with a decrease from 40 °C to 90 °C. After this zone there is no longer rubbery plateau which is replaced by a zone of great instability created by TVAC, as shown in Figure 5c. Moreover, for this adhesive the irradiation exposure does not change the general behavior of E' and E''. The main change concerns the Tg as shown in Table 3. Indeed, initially situated around 91 °C, the latter drops to 72 °C after irradiation and 68 °C after TVAC. As irradiation creates chain splitting and cross-linking which are two opposing phenomena, it is necessary to carry out additional tests to determine which of these phenomena predominates in the adhesives concerned and whether or not they have an impact on the Tg.

3.2 Impact of space conditions on adhesion properties

For DCB test, using DIC (Digital Image Correlation) periodic image recordings, the crack growth is obtained. With these values the opening Mode I interlaminar fracture toughness G_{Ic} is determined using equation (1).

$$G_{I_c} = \frac{3\,P\,\delta}{2b(a+|\Delta|)} \quad (1)$$

Where P is the applied load, a the delamination length, b the width of the DCB specimen, δ the load point displacement and Δ be determined experimentally by generating a least squares plot of the cube root of compliance, as a function of the delamination length using equation (2) as reported in the Modified bean theory (Figure 6).

$$C^{\frac{1}{3}} = \left(\frac{\delta}{\mathrm{P}}\right)^{\frac{1}{3}} \quad (2)$$

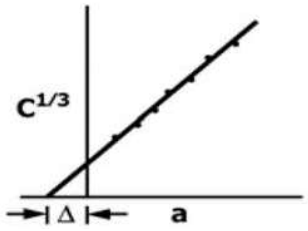

Figure 6: Modified beam theory

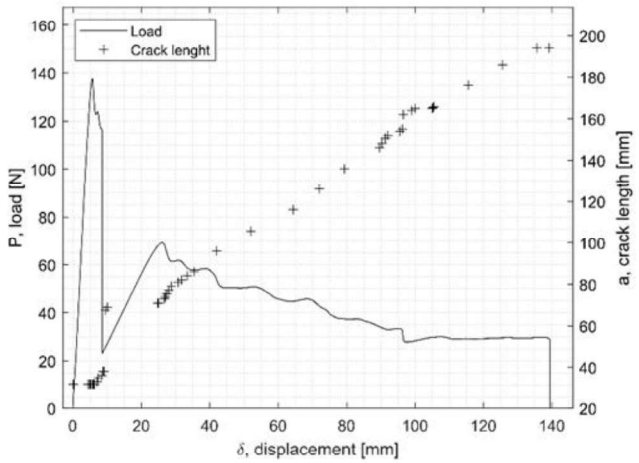

Figure 7: Example of load displacement curve for EC-2216 unaged DCB specimen

Figure 7 shows an example of a load displacement curve as well as the crack growth for EC-2216. Figure 8 shows the evolution of fracture toughness G_{Ic} (R-curve) and the corresponding fracture surface of the specimen.

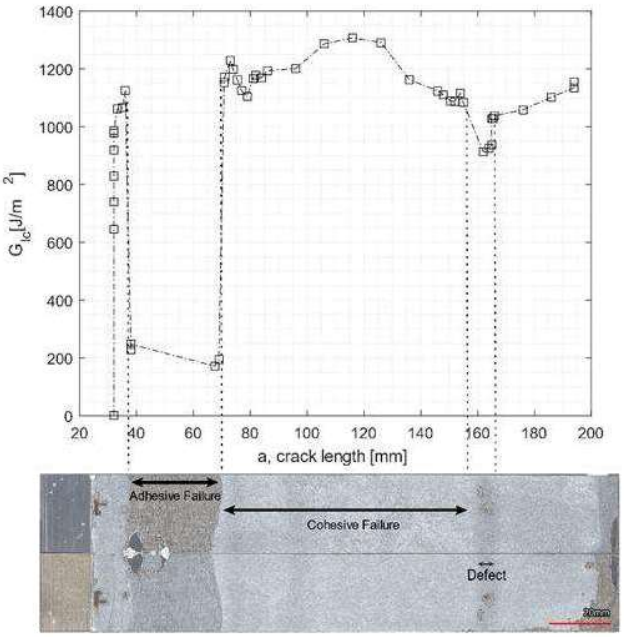

Figure 8: R-curve for EC-2216 unaged DCB sample and the correspondent failure surface of both adherent

From Figure 8 it can be seen that a drop in the value of the fracture toughness corresponds to an adhesive failure. In addition, a second drop in the G_{Ic} appears, due to a change of failure mode created by manufacturing defect, which also cause G_{Ic} drops.

  doi:10.5075/epfl-298799_978-2-9701614-0-0

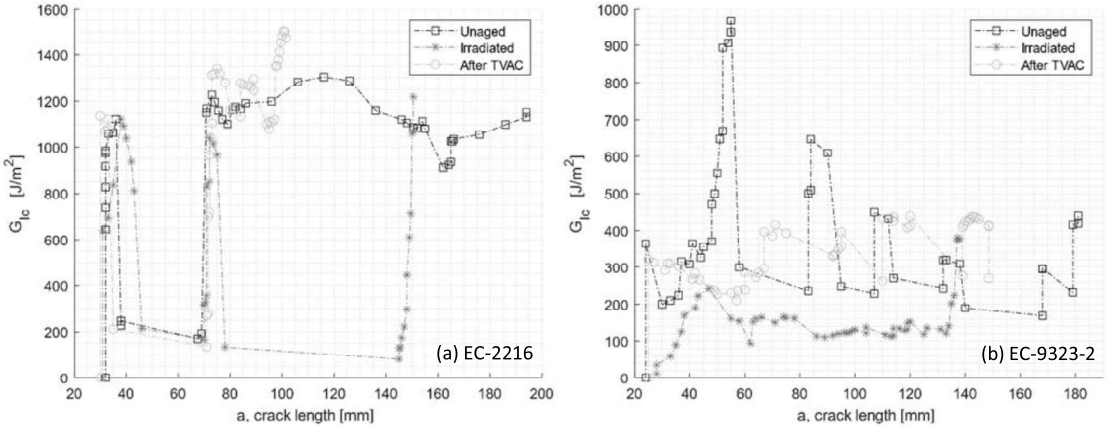

Figure 9: R-curves of DCB test for unaged, after irradiation and after TVAC for (a) EC-2216 and (b) EC-9323-2

Concerning the evolution of the G_{Ic}, the two aging conditions affect differently the adhesives performance. For both adhesives the average value of fracture toughness decreases after particle irradiation. The drop is however more significant for EC-9323-2 with a decrease of almost 50%, while the value of EC-2216 drops by only 5%. In contrast, after TVAC the G_{Ic} value for EC-9323-2 increases by 8% and for EC-2216 by 12% in average. It is interesting to note that TVAC also increased the tested parameters (here fracture toughness) of EC-2216 as it does for the tensile test values. TVAC also increases the G_{Ic}, values for EC-9323-2 but due to significant manufacturing defects in this adhesive samples, the results are less representative than EC-2216.

Table 4: Double Cantilever bean test result with evaluation of cohesive (CF) and adhesive (AF) failure mode

Aging	Scotch-Weld™ EC-2216			Scotch-Weld™ EC-9323-2		
	G_{Ic} [J/m²]	*Failure mode*		*G_{Ic} [J/m²]*	*Failure mode*	
	(on CF)	*CF (%)*	*AF (%)*	*(on CF)*	*CF (%)*	*AF (%)*
Non Aged	1203 ± 52	61 ± 15	39 ± 15	280 ± 100	10 ± 10	90 ± 11
Irradiated	1142 ± 79	41 ± 23	59 ± 23	142 ± 11	0.5 ± 1	100 ± 1
After TVAC	1348 ± 130	31 ± 13	69 ± 13	302 ± 33	0 ± 0	100 ± 0

Concerning the failure type, for EC-2216, both aging processes increase the area of adhesive failure and therefore decrease the proportion of cohesive failure. This means that exposure to space environment related conditions significantly deteriorates the adhesion. For EC-9323-2, the area of adhesive failure also increases. However, samples manufactured with this adhesive have more manufacturing defects.

The floating roller peel test load-displacement curves for unaged, irradiated and post-TVAC conditions are reported in Figure 10. Pictures of the fracture surface of the rigid adherent are displayed below each load-displacement curve. As expected, there is an intimate relation between the peel load and the type of failure. For each of the two surface images, the top

sample is the unaged sample, the middle one is the irradiated sample and the bottom one is the sample subjected to TVAC. In addition, the average peel load values and different failure mode proportions (CF, AF and MD [Manufacturing Defect]) were collected and recorded in Table 5.

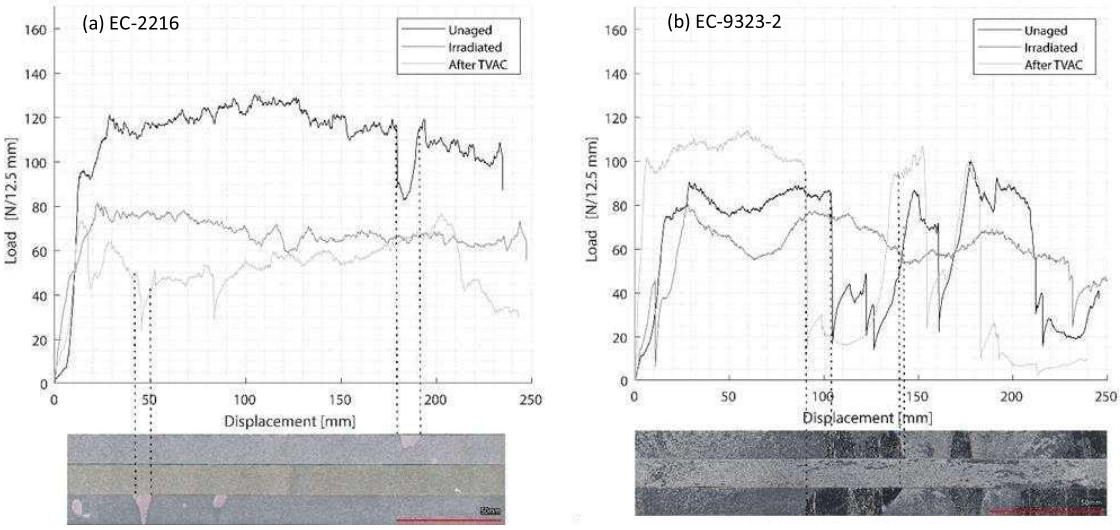

Figure 10: Load displacement curves for peel-test sample non-aged, after irradiation and TVAC for each adhesive and the correspondent failure surface of rigid adherent for (a) EC-2216 and (b) EC-9323-2

EC-2216 shows very few manufacturing defects and a failure 97% cohesive for non-aged samples, which shows the very good quality of the bond line for this adhesive. After radiation of EC-2216, the average peel load decreases by 38% compared to unaged, and after TVAC decreases about 55%. Moreover, irradiation has not significant effect on the failure mode (93 % cohesive failure), however after TVAC, the adhesive failure increases significantly to approx. 30 %. Although results from DCB and tensile tests show that after TVAC for EC-2216, mechanical properties increase, this does not hold true for the floating roller peel tests results.

Table 5: Average peel load and failure mode identification

Aging	Scotch-Weld™ EC-2216				Scotch-Weld™ EC-9323-2			
	F_{ave} [N/12.5 mm]	Failure mode			F_{ave} [N/12.5 mm]	Failure mode		
		CF (%)	*AF (%)*	*MD (%)*		*CF (%)*	*AF (%)*	*MD(%)*
Non Aged	111 ± 6.4	97 ± 2.2	0.8 ± 1.1	2 ± 1.3	87 ± 8	54 ± 27.2	0 ± 0	46 ± 27.2
Irradiated	68 ± 3.5	93 ± 6.1	6 ± 6.5	0.4 ± 0.8	62 ± 5.5	63 ± 23.9	2.2 ± 8	35 ± 26.2
After TVAC	53 ± 6	63 ± 17.7	30 ± 20	7 ± 1.4	105 ± 5	50 ± 7.3	0 ± 0	49 ± 7.3

Figure 11 shows 2D and 3D profile of the rigid adherent of EC-2216, unaged, after irradiation and TVAC. It is shown that after TVAC the adhesive thickness remaining on the rigid adherent part is much higher than for other aging. This indicated the fractured occurred closer to the interface in the case of TVAC than for unaged and irradiation. Indeed, the surface of the

  doi:10.5075/epfl-298799_978-2-9701614-0-0

specimen after TVAC (Figure 10) is slightly pink, which corresponds to the color of the primer applied to the aluminum during the surface treatment. This means that the crack has propagated within the primer and not within adhesive. Peel load values after TVAC are therefore not only representing peel load created by the adhesive but also peel load created by the primer. This value is still quite usable as it qualifies the ability of the sample to resist peeling after thermal aging in vacuum.

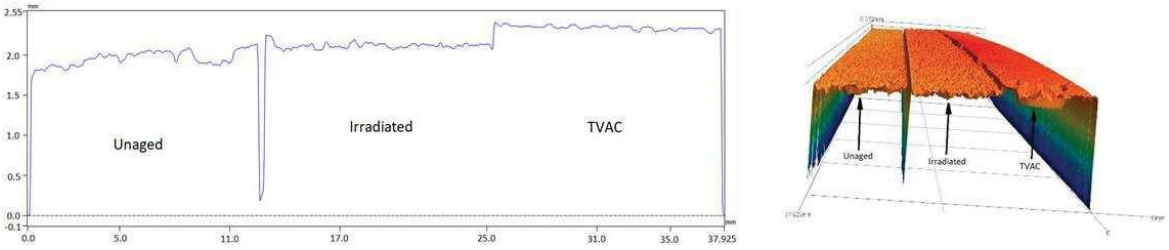

Figure 11: 2D and 3D profiles of EC-2216 thickness present on rigid adherent after testing (unaged on the left, irradiated in the centre and TVAC on the right)

A third failure mode must be considered for peel tests: Manufacturing Defect (MD). The latter is mainly present on EC- 9323-2 specimens. It is represented through a very particular effect on the surface: each of the two faces has adhesive on it, which could suggest a cohesive failure at first sight, but these areas are shiny, which indicates that there has been no bonding between the two faces in this area. The defects are similar to those obtained in the DCB tests with the same adhesive. This reinforces the hypothesis that the entire process used for this adhesive was not optimized specially related to the work life. It was witnessed that during the mixing an exothermic reaction occurs and that the curing reaction starts before the bonding. Thus, the quality of the bond line is reduced.

4. Conclusion

The material properties and adhesion properties to CFRP and to aluminum of EC-2216 and EC-9323-2 under space aging conditions (thermal vacuum and particle irradiation) were evaluated using tensile tests, DMA, DCB tests and floating roller peel tests.

For the Scotch Weld EC-2216 the effect of electron irradiation and thermal vacuum cycling do not influence the Tg. If both cases, decrease in the peel strength occurs with reduction of 50% and 39% for the sample subjected to Thermal vacuum cycling and irradiation, respectively. The DCB test performed using CFRP adherent lead to small increase after TVAC (+12%) and a small decrease after irradiation (-5%) of the G_{Ic}. The tensile properties are positively affected after TVAC with a very strong increase of the modulus and the tensile strength but a decrease of the tensile properties is observed after irradiation.

For Scotch Weld EC-9323-2, the Tg is decreasing after TVAC and irradiation. In both cases, the tensile modulus is negatively impacted with a decrease reaching 50%. TVAC have a positive effect on the G_{Ic} (+8%) value and peel strength (+20%) but a strong negative effect on these values is witnessed after irradiation leading to a decrease of 50% for G_{Ic} and 30% for the peel strength.

The understanding of many of the macroscopic phenomena induced by space environment conditions can be observed and quantified through the results of this study. However, the results on the impact of space aging conditions on the molecular behavior of adhesives do not allow any interpretation. Further detailed study of these behaviors would allow, in addition to the results of this study, to create a predictive model under space aging condition of the degradation of adhesive and adhesion properties. Thus, the durability of the adhesive joints could be quantified enabling lifetime prediction leading to more robust and adequate design and for long-term missions.

Acknowledgements

The authors would like to acknowledge the support of Delft Reactor Institute and ESA-ESTEC for providing access to testing facilities, and of the technical team of the DASML laboratory at TU Delft.

5. References

1. Braunand RD, Manning RM. Mars Exploration Entry, Descent and Landing Challenges 2006; 1.
2. Martin AA. Model Predictive Control for Ascent Load Management of a Reusable Launch Vehicle. Massachusetts Institute of Technology. 2002.
3. Chen J, Ding N, Li Z, Wang W. Organic polymer materials in the space environment 2016; 5.
4. Justiz CR, Sega RM, Dalton C, Ignatiev A. DSMC and bgk-based calculations for return flux contamination of an outgassing spacecraft. Journal of Thermophysics and Heat Transfer 1994; 8:802–803.
5. Laikhtman A, Verker R, Gouzman I, Noter Y, Grossman E. Outgassing effects of a kapton acrylic adhesive tape. Technical report.
6. Zimmermann J, Sadeghi MZ, Schroeder KU. The effect of γ-radiation on the mechanical properties of structural adhesive. International Journal of Adhesion and Adhesives 2019; 93, 9.
7. Dagras S, Eck J, Tonon C, Lavielle D. Adhesives in space environment 2018; 5.
8. Silverman EM. Space environmental effects on spacecraft: Leo materials selection guide. Nasa contractor report 4661. 1995.
9. Stevenson R, Chisabas S, Loureiro G, De Oliveira Lino C, Paola J, Zabala O, Fernando D, Salamanca C. Development of a thermal-vacuum chamber for testing in small satellites. 2017.
10. Teixeira de Freitas S, Banea MD, Budhe S, de Barros S. Interface adhesion assessment of composite-to-metal bonded joints under salt spray conditions using peel tests. Composite Structures 2017 ; 164:68–75, 3.
11. Teixeira de Freitas S, Zarouchas D, Poulis JA. The use of acoustic emission and composite peel tests to detect weak adhesion in composite structures. Journal of Adhesion 2018; 94:743–766, 7.
12. Lee-Sullivan P, Dykeman D. Test method guidelines for performing storage modulus measurements using the TA instruments DMA 2980 three-point bend mode 1 amplitude effects. 2000.
13. Teixeira De Freitas S, Sinke J. Adhesion properties of bonded composite-to-aluminium joints using peel tests. Journal of Adhesion 2014; 90(5-6):511–525, 6.
14. Benzarti K, Chataigner S, Quiertant M, Marty C, Aubagnac C. Accelerated ageing behaviour of the adhesive bond between concrete specimens and CFRP overlays. 2010.
15. ASTM D638. Standard test method for tensile properties of plastics. 2014.

16. ASTM D7028. Standard test method for glass transition temperature of polymer matrix composites by dynamic mechanical analysis. 2015.
17. ASTM E2254. Standard test method for storage modulus calibration of dynamic mechanical analyzers. 2018.
18. ASTM E2425. Standard test method for loss modulus conformance of dynamic mechanical analyzers. 2016.
19. ASTM D3167. Standard test method for floating roller peel resistance of adhesives. 2017.
20. ASTM D5528. Standard test method for mode 1 interlaminar fracture toughness of unidirectional fiber-reinforced polymer matrix composites. 2013.
21. Huang G, Ni Z, Chen G, Zhao Y. The influence of irradiation and accelerated aging on the mechanical and tribological properties of the graphene oxide/ultra-high-molecular-weight polyethylene nanocomposites. 2016.
22. Sahu SK, Badgayan ND, Samanta S, Rama Sreekanth PS. Dynamic mechanical thermal analysis of high-density polyethylene reinforced with nanodiamond, carbon nanotube and graphite nanoplatelet. Materials Science Forum 2018; 917:27-31.
24. Williamson JR, Semprimoschnig C, Simon-Boutemen P, Levan L, Van Eesbeek M. Use of model free kinetic lifetime values to evaluate mechanical performance of a high temperature polyimide composite. Proceeding of 11th ISME 2009
25. Space product assurance adhesive bonding for spacecraft and launcher applications. ECSS-Q-ST-70-16C ESA-ESTEC requirements and standards section. 2020.
26. ASTM D3418. Standard Test Method for Transition Temperatures and Enthalpies of Fusion and Crystallization of Polymers by Differential Scanning Calorimetry. 2021

